

# Tactile Discrimination using Active Whisker Sensors

J. Charles Sullivan, Ben Mitchinson, Martin J. Pearson, Mat Evans, Nathan F. Lepora, Charles W. Fox,  
Chris Melhuish and Tony J. Prescott

**Abstract**—We describe a novel, biomimetic tactile sensing system modeled on the facial whiskers (vibrissae) of animals such as rats and mice. The “BIOTACT Sensor” consists of a conical array of modular, actuated hair-like elements, each instrumented at the base to accurately detect deflections of the shaft by whisker-surface contacts. A notable characteristic of this array is that, like the biological sensory system it mimics, the whiskers are moved back-and-forth (“whisked”) so as to make repeated, brief contacts with surfaces of interest. Furthermore, these movements are feedback-modulated in a manner intended to emulate some of the “active sensing” control strategies observed in whiskered animals. We show that accurate classification of surface texture using data obtained from whisking against three different surfaces is achievable using classifiers based on either naive Bayes or template methods. Notably, the performance of both these approaches to classify textures after training on as few as one or two surface contacts was improved when the whisking motion was controlled using a sensory feedback mechanism. We conclude that active vibrissal sensing could likewise be a useful sensory capacity for autonomous robots.

## I. INTRODUCTION

An important characteristic of many biological sensory systems is that they are active, where “active” here means purposively controlled and information-seeking in the sense described by Bajcsy [1], rather than operating by emitting energy (which is an alternative meaning for the phrase “active sensing”). An example of biological active sensing, in the realm of touch, comes from the way we control the movement of our hands and fingers depending on the type of information about a surface or object of interest that is being sought. For instance, we typically stroke a surface with our fingertips to determine texture, palpate at different locations to judge shape, and press or squeeze to assess hardness [2]. In this article we discuss biomimetic tactile sensing in the context of a different, but perhaps equally important, active sensory system – the facial whiskers (or vibrissæ) of mammals. Nearly all mammals have facial whiskers but the specialists in vibrissal sensing, such as rats and mice, tend to be creatures of small body-size living nocturnally, or in environments with limited natural light, who will use their whiskers in support of locomotion, navigation, prey catching, and even social behavior [3]. Vibrissal sensing is of interest to engineers as artificial vibrissae could provide proximal sensors that can determine distance to nearby objects alongside surface characteristics such as shape and texture [4]). A useful property is that vibrissal sensors could be employed in circumstances where the efficacy of other types of proximal sensing could be seriously compromised – for instance in environments containing smoke or dust,

or in darkness where there is a need to operate covertly.

The biomimetic vibrissal sensing system described in this article has been developed as the result of a long-term collaboration between biologists and engineers aimed at advancing the understanding of biological vibrissal systems and determining to what extent, and in what forms, vibrissal sensing could be useful in engineered systems such as autonomous robots. Most recently this collaboration has taken the form of a European Framework 7 project termed BIOTACT (BIOmimetic Technology for vibrissal Active Touch), and in this article we describe the design of a vibrissa-based sensory array – the BIOTACT sensor – that has been one of the chief focuses of that project. The BIOTACT sensor is the latest in a line of artificial vibrissal systems (see [4], [5]) modelled most directly on that of the common rat. We have taken inspiration from this animal model in various ways, investigating and attempting to mimic aspects of: (i) vibrissal morphology including the physical characteristics of individual whiskers and their organisation into a spatial-distributed array of different length elements; (ii) vibrissal control including the manner in which the whiskers are moved and positioned both through actuation of individual whiskers and through the ability to orient the full array; and (iii) vibrissal sensory processing including analysis of the types of tasks in which vibrissal sensing is employed by animals and the nature of the information they are thought to extract from vibrissal signals. In this article we consider each of these different areas of potential biomimicry. In each case we briefly describe some of the salient characteristics of biological vibrissal systems, discuss how these have influenced the design of our artificial sensor, and show how the current sensor prototype implements key properties of interest. We also describe a number of experiments with this prototype showing, in particular, how we have implemented biomimetic vibrissal control, and how properties, such as surface texture and radial distance to contact, can be extracted from sensor signals. In the discussion we consider the impact of active control on the information-gathering capacities of our novel sensor in the context of our twin goals of furthering the understanding of biological vibrissal sensing and developing useful artificial vibrissal sensors for robotics. Finally we outline some of the limitations of our current sensor design and describe how these might be overcome in the future.

## II. THE BIOTACT SENSOR

### A. The Whisking System in Rat

Long facial whiskers, or *macrovibrissæ*, are found in many mammalian species, projecting outwards and forwards from

the snout of the animal to form a tactile sensory array that surrounds the head (see [6], and Figure 1). In rats, the macrovibrissæ form a two-dimensional grid of five rows on each side of the snout, each row containing between five and nine whiskers ranging between  $\sim 15\text{mm}$  and  $\sim 50\text{mm}$  in length. Each whisker is mounted in a specialised and mechanically complex hair follicle (see [7] for a description). These, in turn sit within an area of dense muscular tissue strongly innervated by nerve fibres called the mystacial pad. From an engineering perspective facial whiskers can be thought of as tapered elastic beams that deform easily upon contact with objects, and possibly also as the result of movement through air. Since the whisker shaft is composed of dead hair cells, the transduction of whisker deformations into neural activity begins inside the follicle where multiple populations of mechanoreceptors surround the base of the shaft and respond with high acuity when it is deflected. Mechanoreceptor responses are then transduced into patterns of neural firing in approximately 200 primary afferent fibres (per whisker) within the facial nerve. This transduction apparatus has been found to respond, in different ways, to rotation of the follicle by its muscles and deflection of the whisker shaft by external contacts. Thus activity in facial nerve neurons is thought to encode information about the direction, velocity, and duration of whisker displacements.

When the rat is moving and exploring its surroundings the long facial whiskers are swept back and forth, at typical rates of seven to ten “whisks” per second [8]. The forward and backwards motion of each vibrissa is partly determined by its own intrinsic muscle, and partly by a set of extrinsic muscles that anchor the mystacial pad to the bones of the skull. Thus although each whisker has some capacity for independent movement, the whiskers on each side of the snout generally move together, coupled by linkages within the pad and by the action of extrinsic muscles.

In addition to the macrovibrissæ, rats also have a large number of shorter, more densely packed, and non-actuated microvibrissæ on the chin and lips. These arrays of short whiskers are thought to form the “fovea” of the vibrissal system [9] being brought to bear on objects and surfaces by head and body orienting movements triggered when the longer whiskers make unexpected contacts.

### B. Sensor Design

The G1 (Generation 1) BIOTACT sensor consists of a truncated conical “head” made from ABS plastic, which holds up to 24 whisker modules. The whisker modules are arranged in 6 radially symmetric rows of 4 and are oriented at outward-facing normals to the cone surface. For the purposes of our experiments and to enable accurate and repeatable location and movement of the sensor, it is mounted as the end-effector of a 7 degree of freedom robot arm (figure 2 shows the G1 sensor fitted with 8 whiskers). Also, for the experiments reported here, the head was not fully populated with whiskers. Two rows were fitted with 3 whiskers each to create a bilaterally symmetric configuration.



Fig. 1. Rat facial whiskers (*vibrissae*)

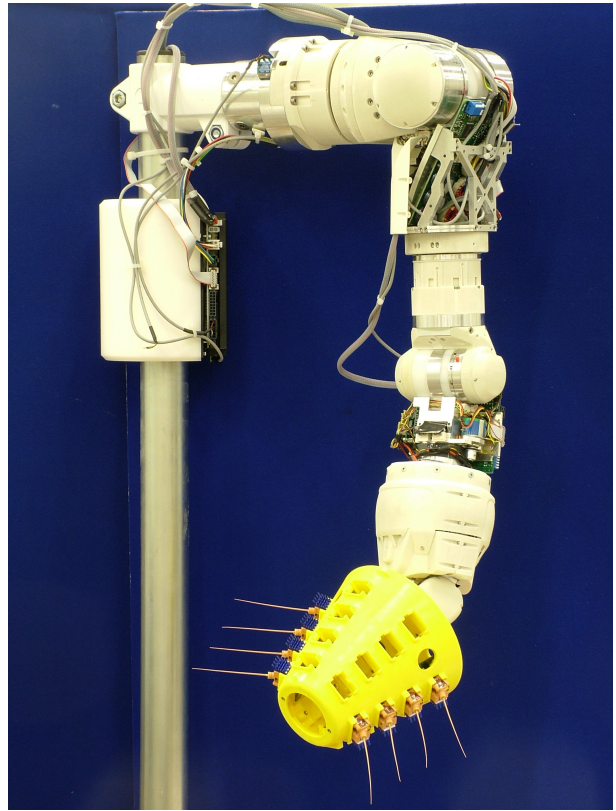


Fig. 2. The BIOTACT G1 Sensor Head and Robot Arm

### C. Design of Active Whisker Sensor Module

The individual whisker sensors are completely modular in design, incorporating their own actuation mechanism and control electronics. Actuation is by means of miniature brushless DC motors (Faulhaber 1307BH) which incorporate an 11:1 gearbox, controlled by custom-built three-phase bridge drivers, with closed-loop PD control provided by on-board microcontrollers (Microchip dsPIC33FJ128GP802). The modules are 20mm by 15mm by 15mm in size (see figure 3) and weigh 8 g including the controller boards. Typical power consumption during whisking is 0.4W. They are capable of whisking at frequencies of up to 10 Hz which is roughly comparable to the whisking rate of real rat mystacial whiskers [10].

Software to process the signals from the whisker sensors and to control the whisking patterns is written in C++ and executed under the BRAHMS Modular Execution Framework [11] on a PC which connects to the sensor head via a USB2 connection, running in high speed bulk transfer mode. This is able to transmit data to and from the sensor (half-duplex) synchronously at  $500\mu\text{s}$  intervals, enabling data transfer and feedback updates at 2kHz.

The whisker sensor is based on the principle of Hall-effect detection of movement of a small magnet fixed to the base of the whisker. Monolithic tri-axis Hall effect sensor ICs by Melexis (MLX90333) are used and these incorporate two orthogonal pairs of Hall plates which, together with on-chip signal processing, enable the three orthogonal components of magnetic field strength, to be resolved with 14 bit resolution. These data, together with the protraction angle ( $\theta$ ) of the whisker relative to the head are sent in synchronous serial form using an SPI bus to the local microcontroller. Data from the microcontrollers are collected via six separate SPI busses which are marshalled by an FPGA (Xilinx Spartan 3e) and then sent to the FIFO buffer of the USB controller (Cypress FX2). The FPGA acts as the bus master for the SPI busses and data transfers in packets of 512 bytes are synchronised with the USB2 host controller on the PC resulting in very low latency and jitter.

The whiskers are made using a DLP (Data Light Processing) rapid-prototyping machine (Envisiontec Perfactory) in Nanocure RC25, a composite material consisting of a UV-curing photo-polymer matrix and aluminium oxide nanoparticle filler. The combination of the DLP process and the composite material enable us to make whiskers which taper to a fine point (0.25mm diameter) and yet retain sufficient strength and toughness to withstand repeated impact against the discriminanda. Two important benefits of whisker taper, and in particular the fine tip diameter were highlighted in [12]: a small tip should improve resolution of fine surface features (here we are attempting to discriminate surface textures with mean particle diameters of  $25\mu\text{m}$ ) and tip breakages (which are common for real rat whiskers) have a smaller effect on natural frequencies of vibration. The artificial whiskers have a taper ratio (hub/tip) of 8, whereas rat whisker taper ratios are typically 10–20 with tip diameters of  $\sim 10\mu\text{m}$ . Rat whiskers are both tapered and curved but we have chosen not to mimic the curvature of the natural whiskers in these experiments. Future work will examine the effect that curvature has on the ability to discriminate texture.

Note also that the whisker lengths in the test configuration were not all the same: they increased from front to rear in order that all whiskers could touch a plane surface orthogonal to the axis of the cone (see Figure 4). This feature was also motivated by the observation that the whiskers within each row of the mystacial pad of rats and other whisking mammals closely follow an exponential increase in length from the front to the rear: the actual ratio of length between adjacent whiskers is species and row specific, varying from 1.2 to 1.6 [9]. In our experiments we used whiskers of length 80mm, 112mm and 158mm, corresponding to a ratio of 1.4. Our whiskers were longer than those of whisking mammals, which

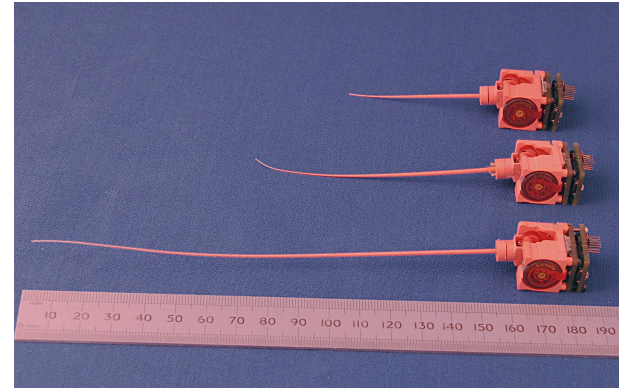


Fig. 3. Whisker Modules

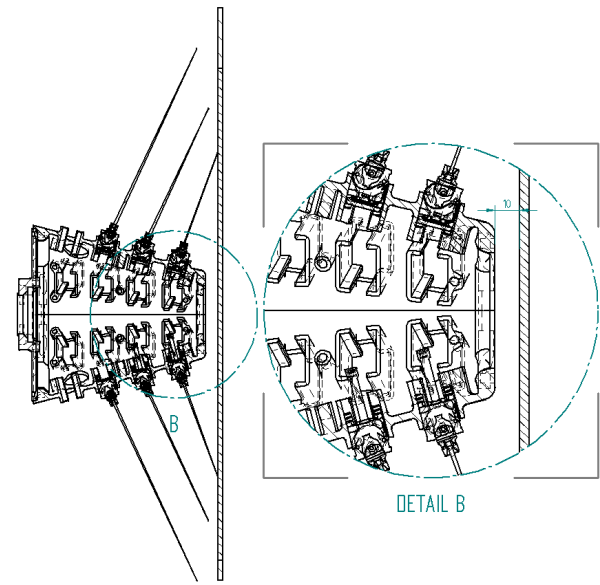


Fig. 4. G1 Sensor in Test Configuration (section)

in rats are typically between 15mm and 50mm long [3]. The lowest static natural frequencies of vibration of the artificial whiskers were measured in-situ, using Fourier spectral analysis of response after release from an imposed deflection parallel to the motor axis, as 86Hz, 50Hz and 21Hz respectively. Frequencies of corresponding whiskers on each side were within 1Hz. Studies of the mechanical characteristics of rat whiskers have revealed that they have natural frequencies in the same range. Hartmann et al. [13] for example, measured frequencies between 27Hz and 260Hz, noting that in all cases whisker resonant frequencies were significantly higher than the whisking frequency.

### III. MOTOR CONTROL

#### A. Motor Control in Rats

Although early research emphasized the regularity and symmetry of whisker motion (e.g. [14]), more recent work by the current authors, and in other laboratories, has shown that biological whisker motion is often strongly modulated by the nature of the task [15], by the intentions of the animal [16], and by the immediate environment [17], [18].

It has been hypothesized (for example, see [17]) that some of these modulations are functional, and more specifically, that they are examples of ‘active sensing’ control, serving to improve the quality and/or quantity of sensory information collected. The BIOTACT sensor is an ideal platform for testing these hypotheses: its great number of degrees of freedom allow the comparison of the impact of different motor control strategies on data collection. In the current article we focus on two candidate active sensing strategies, termed rapid cessation of protraction (RCP), and contact-induced asymmetry (CIA).

The forward and backward phases of the periodic ‘whisking’ motions, observed in rats and mice, are usually denoted protraction and retraction, respectively. RCP is the observation that when the animal’s whiskers encounter a novel object they often do so with a relatively ‘light touch’; that is, the forward protraction of the whiskers stops very soon (12–14 milliseconds) after the initial contact preventing strong bending of the whiskers against the surface. This was first observed by Mitchinson et al. [17] in the situation where the animal encounters an object on one side of the snout only (Figure 5). Here, whisker motion on the ipsilateral (i.e. contacting) side of the snout can be seen to cease shortly after the contact, whilst protraction on the contralateral (opposite first contact) side continues seemingly unaffected by the surface impact. Grant et al. [18] went on to show that RCP takes place even when whiskers on both sides of the snout contact the surface and that it occurs in the second whisk cycle following the initial contact as well as in the first (and probably also in subsequent whisk cycles where there is continued contact). Interestingly, one effect of RCP can be to break the synchrony of the whisker movements in the left and right fields, potentially leading to extended periods where the whiskers on the two sides of the face move asynchronously (unpublished observations). RCP is an example of feed-back control, since the sensory signals resulting from whisker-environment contact are used to regulate the same contact.

CIA is the related observation that when an animal has made contact with a nearby vertical surface the whiskers on the two sides of the snout are observed to move asymmetrically in subsequent whisks in advance of any further contact. Specifically, whiskers in the ipsilateral (nearest to surface) field tend to protract less, whilst the contralateral whiskers (furthest away) are seen to protract more strongly (Figure 5). The result is, again, on the ipsilateral side, to allow the whiskers to make light contacts with the surface avoiding strong bending, whilst on the contralateral side the increased protraction tends to lead to more whisker contacts with the surface. CIA, in contrast to RCP, is an example of feed-forward control, since the sensory signals resulting from contact during one whisk are used to regulate contacts occurring during subsequent whisks.

Observationally, whisking behavior thus appears to be consistent with a ‘minimal impingement, maximal contact’ active control strategy [17], where ‘impingement’ describes the extent to which the whiskers could be imagined to penetrate through the contacted surface if it were to offer no resistance. A further observed modulation of whisking, consistent with the maximal contact element of this hypothesis, has been described by Grant et al. [18]. This is the ability of the animal

to differentially control the velocity of the forward and rear whiskers, and thus the angular separation or ‘spread’ of the whiskers, in order to bring the rear whiskers further forward and (again) increase the number of contacts with the surface of interest.

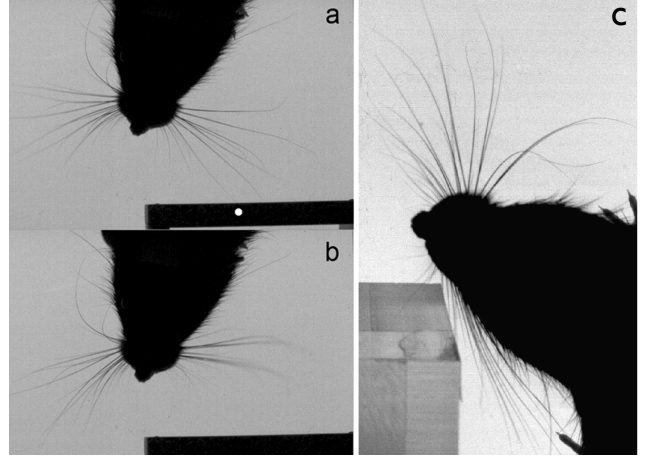


Fig. 5. Snapshots from high-speed videography recordings of rat whisker movement. (a, b). An example of rapid cessation of protraction (RCP). In (a) the left and right whisker fields are protracting synchronously when one of the forward whiskers in the ipsilateral (left-hand) field makes contact (indicated by the white dot) with a vertical surface. Protraction on the ipsilateral side ceased 12 msec later whilst protraction continued contralaterally (adapted from [17]). In (b), 32 msec after the contact, the ipsilateral whiskers are already considerably retracted when the contralateral field reaches maximum protraction. (c). An example of contact-induced asymmetry (CIA). Here, the whiskers ipsilateral (nearest) to the Perspex block can be seen to be considerably less protracted than those contralateral (image from the Active Touch Laboratory).

In the following sub-sections we describe first our implementation of bilateral whisking pattern generation for the BIOTACT sensor using two coupled oscillators. We then describe how this is modulated by vibrissal signals to generate RCP and CIA that is functionally similar to that observed in the animal (n.b. we make no strong claim concerning the similarity of the underlying mechanisms). Although a number of active sensing strategies have been demonstrated on our earlier whiskered robot platforms [19]–[22], we have not previously investigated or measured the consequences of this active control for sensory discrimination. Our first efforts to do this using the BIOTACT sensor are described in Section IV.

### B. Pattern Generation Model

Whisking, as described above, consists most simply of periodic forward and backward motion, and this is what we reproduce first using the BIOTACT Sensor. In the animal, it has been shown that the motion is generated by a Central Pattern Generator (CPG), an intrinsic oscillator that does not require connection to the environment to operate [14]. Since it is known that periodic whisking that is out-of-phase on the two sides of the animal may be expressed, at least two such oscillators must be present. However, whisking tends towards being in phase, so these oscillators must be coupled. In addition, the oscillators may be perturbed by extrinsic events.

We model two individual oscillators, each as a two-dimensional dynamical system with a time-dependent state

$\Psi_i$ . The state can be alternatively written as follows (time dependence is not explicitly shown in most of the equations below, for notational simplicity).

$$\Psi_i = \begin{bmatrix} \psi_{i,1} \\ \psi_{i,2} \end{bmatrix} = \begin{bmatrix} r_i \cos(\phi_i) \\ r_i \sin(\phi_i) \end{bmatrix} \quad (1)$$

The subscript  $i$  is chosen from 1, 2 and indexes into the pair of oscillators (also denoted ‘left’ and ‘right’). The update equation is given by

$$\frac{d\Phi_i}{dt} = D_i + C_i + P_i \quad (2)$$

where the three terms on the right hand side represent the forcings due to, respectively, the oscillator characteristic, the coupling between the two oscillators, and any perturbation of the oscillator caused by extrinsic events. Integration is forward Euler with an integration period  $T$  and, for physical plausibility, all  $\psi$  states are hard limited to fall between plus and minus  $\psi_{\text{lim}} = 1.5$  after the computation of each timestep.

The update representing the dynamics is given in polar space for simplicity, as follows.

$$D_i^{\text{polar}} = \begin{bmatrix} (1 - r_i)/\tau_r \\ 2\pi f_W \end{bmatrix} \quad (3)$$

This represents a system with a limit cycle on the unit circle and a period of  $1/f_W$  seconds. The whisking frequency is set to  $f_W = 2$  throughout this report; we also define the whisk period,  $T_W = 1/f_W$ . Also throughout, we use  $\tau_r = 2T_W$ . The coupling forcing is given in cartesian space, as follows

$$C_i = \begin{bmatrix} (\psi_{j,1} - \psi_{i,1})/\tau_{11} + (\psi_{j,2} - \psi_{i,1})/\tau_{12} \\ (\psi_{j,1} - \psi_{i,2})/\tau_{21} + (\psi_{j,2} - \psi_{i,2})/\tau_{22} \end{bmatrix} \quad (4)$$

where  $j = 3 - i$  is the index of the opposite oscillator and  $\tau_{pq}$  is the time constant with which state  $\psi_{i,p}$  is forced towards state  $\psi_{j,q}$  of the opposite oscillator. Note that a negative  $\tau_{pq}$  will tend to force states apart. In this report, only  $\tau_{11}$  is not infinite (that is, only the first coupling term is non-zero), and it always takes a positive value of  $2T_W$ , which brings the oscillators back into phase with a time constant of one whisking period.

In this report, the only perturbation is a noise signal, given by the following.

$$P_i = \begin{bmatrix} \sigma_\eta H_{50}(\eta_{i,1}) \\ \sigma_\eta H_{50}(\eta_{i,2}) \end{bmatrix} \quad (5)$$

$\eta_{i,d} \sim N(0, 1)$  is White Gaussian Noise,  $H_{50}$  is a third-order lowpass Butterworth filter with 50Hz cutoff frequency, and  $\sigma_\eta = 0.005$  is a small noise amplitude. The first state of each oscillator,  $\psi_{i,1}$ , is associated with whisker protraction on that side by deriving a ‘muscle drive’ signal from it as follows.

$$W_i = \frac{\tanh(2\psi_{i,1}) + 1}{2} \quad (6)$$

The other state  $\psi_{i,2}$  can be viewed as the recovery state of the oscillator, and its value does not affect any output.  $W_i$  is used to drive a mechanical model of the motion of the whiskers, as follows.

$$m \frac{d^2\theta_{i,w}}{dt^2} = q_{i,w} W_i - k\theta_{i,w} - \nu \frac{d\theta_{i,w}}{dt} \quad (7)$$

$m = f_W^2/100$  is a mass,  $k = 1$  is a spring constant and  $\nu = 4\sqrt{km}$  a damping constant. Hence,  $\theta_{i,w}$ , the protraction angle of the  $w$ th whisker on the  $i$ th side, displays second-order dynamics in response to the muscle drive  $W_i$ .  $q_{i,w}$  is the muscle gain (coefficient between drive and force) associated with the  $w$ th whisker on the  $i$ th side, and is given by the following equation.

$$q_{i,w} = 1.45(1 - z_i)g_{i,w}e^{-\theta_{i,w}^2} \quad (8)$$

$z_i \in [0, 1]$  is a gating variable associated with the  $i$ th side. It takes a nominal value of zero (no suppression), and can range up to one (total suppression), modelling suppression of muscle drive to all whiskers on that side.  $g_{i,w} \in [0, 2]$  is a gating variable associated with the  $w$ th whisker on the  $i$ th side, which controls how excitable the individual whisker is – i.e. how much the whisker responds to the drive from the oscillator. It takes a nominal value of one, and can range both positively and negatively, modelling excitation or suppression for each whisker individually. The constant term scales the overall gain so that with  $z_i = 0$  and  $g_{i,w} = 2$ ,  $\theta$  approaches, but does not exceed, unity (see below). The final (exponential) term is a simple model of the reduction in force produced by a muscle as its length decreases (reaching 37% as  $\theta$  reaches its maximum value of unity). The overall effect is that the values of  $z_i$  and  $g_{i,w}$  control the response of each side and each whisker, affecting both amplitude of oscillation and mean protraction angle, although it should be noted that there is no direct independent control over these latter variables.

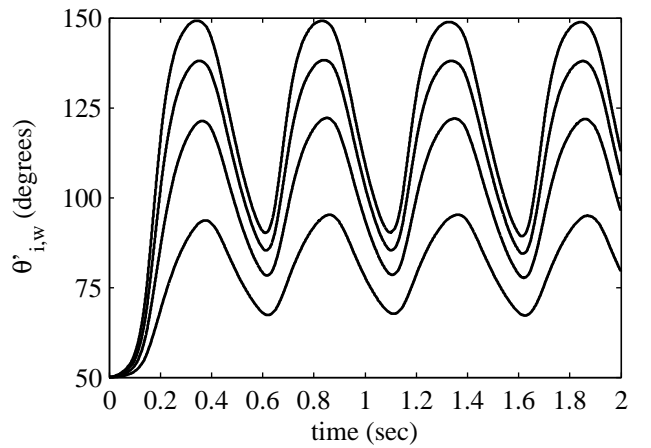


Fig. 6.  $\theta'_{1,1}$  during free (unperturbed) whisking with four different values of  $g_{1,1}$  (higher values generate higher values of  $\theta'_{i,w}$ ).

An example of the effect of varying the gain is given in Figure 6. The output, the angle of the first whisker on the left side, is given for  $z_1 = 0$  and  $g_{1,1} \in \{0.5, 1.0, 1.5, 2.0\}$ .  $\theta' = 100\theta + 50$  is plotted, which is the conversion of  $\theta$  (which ranges in zero to one) into an angle in degrees to pass to the motor hardware.

### C. Rapid Cessation of Protraction

A substantial component of whisker motor control that has been quantified is the *Rapid Cessation of Protraction* (RCP) that often follows contact between the whiskers and the environment, and which is hypothesised to limit the degree to which the whiskers bend during contact [17], [18]. We wish to reproduce this aspect because controlling the degree of bending could potentially improve the quality of data collected.

A contact signal is derived on each side from the  $x$ -deflection of the whiskers on that side (contact usually elicits strong  $x$ -deflection since the sensory  $x$ -axis is parallel to the actuated axis). A third-order lowpass Butterworth filter with 50Hz cutoff frequency,  $H_{50}$ , is first used to smooth the noisy whisker sensory signals. The maximum absolute value of this signal, across all whiskers on a side, forms the contact signal,  $\pi_i$ .

$$\pi_i(n) = \max_{w \in [1,12]} |H_{50}(x_{i,w}(n))| \quad (9)$$

This signal is used to suppress protraction ipsilaterally, through the gating variable  $z_i$ , without affecting the oscillator dynamics. The gating variable dynamics are given by

$$z_i(n) = \langle \max((1 - T/\tau_z)z_i(n-1), \sigma_z \pi_i(n)) \rangle_0^1 \quad (10)$$

where  $\sigma_z$  is a gain associated with the motor modulation, and  $\langle \cdot \rangle_a^b$  is a limit operation (transforming values not in the interval  $[a, b]$  onto the nearest value that is in the interval). Contact on any whisker, thus, suppresses protraction ipsilaterally, an effect which decays with time constant  $\tau_z$ . We can simply simulate contact signals from the whisker sensors using the following equation.

$$x_{i,w} = \langle \sigma_x \max(0, \theta'_{i,w} - \theta'_{i,\text{lim}}) \rangle_{-1}^{+1} \quad (11)$$

We simulate an obstruction at a different location on each side by setting  $\theta'_{1,\text{lim}} = 100$  and  $\theta'_{2,\text{lim}} = 125$ , using  $\sigma_x = 0.1$ . Setting  $\sigma_z = 0.7$  and  $\tau_z = T_W/4$  generates the results graphed in Figure 7. Protraction on the contacting (left) side is suppressed during contact, such that the depth of contact is controlled. The oscillator dynamics are unaffected, so the phase behaviour is unchanged. Furthermore, the gating variable  $z_1$  has all but recovered by the time of the next contact, so there is no inter-whisk modulation; that is, this aspect of control is entirely *reactive*.

We can simulate stronger and faster RCP control by setting  $\sigma_z = 2$  and  $\tau_z = T_W/10$ ; the results are shown in Figure 8. In this case, protraction is more strongly suppressed such that the  $\theta_{1,w}$  quickly fall below  $\theta_{1,\text{lim}}$  and the contact signal  $\pi_i$  becomes zero. Thus, the gating variable  $z_1$  quickly recovers, and protraction reignites within the same whisk period, resulting in a biphasic whisk profile. We hypothesise that this control loop may be the origin of the biphasic whisks that have been observed in whisking animals [23].

Note that in the experiments presented in section IV we have set  $\tau_z$  to  $T_W/4$  throughout and the maximum value of  $\sigma_z$  was 0.9 so that this biphasic whisking was not encountered.

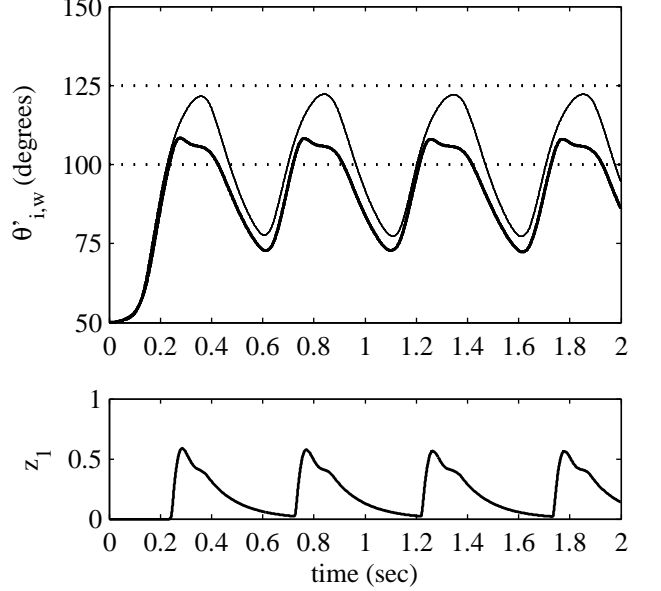


Fig. 7. Whisking with RCP modulation. When the left whiskers (thick line) are driven past a simulated obstacle (lower dotted line), a contact signal results which temporarily excites the gating variable  $z_1$  and suppresses protraction ipsilaterally. The right whiskers (thin line) do not reach the obstruction on that side (upper dotted line), and are not modulated (thus, they show the expected movement of the left whiskers if the modulation were absent).

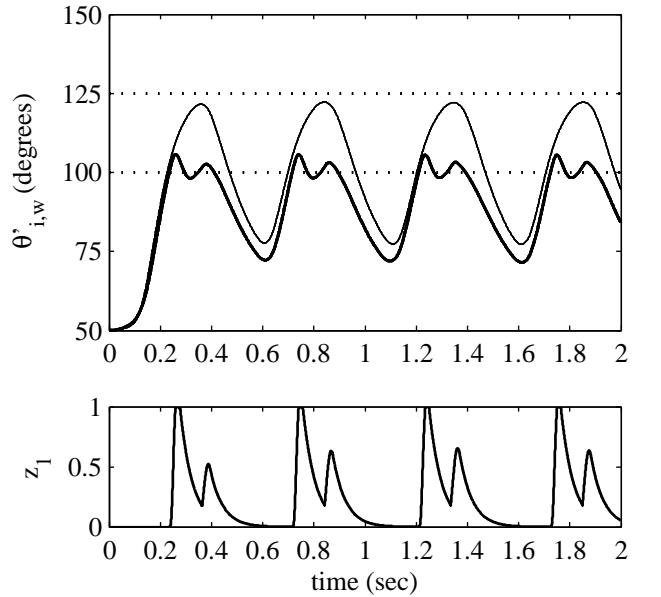


Fig. 8. Whisking with strong and fast RCP modulation. Left whiskers (thick line) quickly detach from the simulated obstacle (lower dotted line), and protraction reignites within a single whisk, leading to a biphasic whisk profile and two distinct contacts with the obstacle. The movement of the right whiskers (thin line) shows the expected movement of the left whiskers if the modulation were absent.

### D. Contact-Induced Asymmetry

Another aspect of whisker motor control that has been measured is *Contact-Induced Asymmetry* (CIA), in which contact with a unilateral obstruction has been shown to reduce/increase whisker protraction on the ipsilateral/contralateral side [17], [18]. Here, we model CIA by introducing global excitation

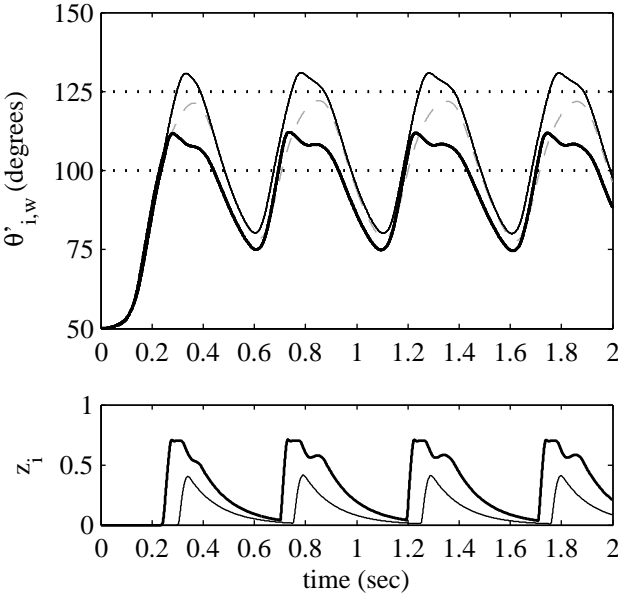


Fig. 9. As Figure 7, but with CIA modulation enabled as well as RCP modulation. The left whiskers (thick solid line) contact an obstruction (lower dotted line) first, and cause excitation of the gating variables  $g_{i,w}$ , leading to global excitation of protraction. Thus, the right whiskers (thin solid line) are pushed forward and ‘find’ the obstruction on the right side (upper dotted line) – compare with Figure 7, where the obstruction on the right side is not found. Since both sides are modulated, here, we show also (dashed gray line) the expected movement of both sides were the modulations absent.

of protraction in all whiskers following contact, through the gating variables  $g_{i,w}$ . CIA results from the interaction of this global excitation with the reduction of protraction on the ipsilateral side due to the RCP mechanism described above.

The dynamics of  $g_{i,w}$  are governed by the equations below. The results of using this modulation with  $\sigma_g = 0.5$  and  $\tau_g = T_W/4$  ( $\sigma_z = 0.7$ ,  $\tau_z = T_W/4$ , as for Figure 7) are shown in Figure 9. The whiskers on the right side are now brought forward and ‘find’ the obstruction.

$$g_{i,w}(n) = \langle \max(g_{i,w}^*(n), \sigma_g \zeta(n)) \rangle_0^2 \quad (12)$$

$$g_{i,w}^*(n) = g_{i,w}(n-1) + T/\tau_g(1 - g_{i,w}(n-1)) \quad (13)$$

$$\zeta = \max(\pi_1, \pi_2) \quad (14)$$

### E. Summary

In summary, the motor control strategies described in this section may help the robot, in emulation of the rat, to take best advantage of its sensors (whiskers) in the face of the changing geometry of its near environment (Figures 5 and 9). Complete quantification of the impact of these strategies in different sensory tasks will require extensive testing. In the following section, we present our first assessment of the impact of implementing RCP, measuring the effect on performance in a texture discrimination task.

## IV. SENSORY DISCRIMINATION

### A. Sensory Discrimination in Rats

Experiments with rats (reviewed in [3], [24]), and with other tactile specialists such as the Etruscan shrew [25], have shown that whiskered animals are able to use their facial vibrissae to localise objects in space and to discriminate object properties such as shape and texture. For instance, in localisation tasks, rats have been shown to use vibrissal information in gap measurement and gap jumping, and to be able to measure angular position of a contact along the sweep of the whisker, and the axial distance to a point of contact on a single whisker. Ahissar et al. [26] have proposed that the timing and extent of bending of the whiskers together provide sufficient information to localise a point of contact in 3d space (elevation, azimuth, and axial distance, respectively). Several studies have shown that rats can use their macrovibrissae to reliably discriminate between surfaces with different texture, showing a similar level of acuity to human fingertips [10], [27], [28]. Movement of an individual whisker across a texture has been shown to give rise to a characteristic whisker vibration or “kinetic signature” which is thought to form the basis on which sensory discriminations are made [24], [29], [30], although the precise process that underlies such discriminations is not well understood.

A number of studies with artificial whiskers have looked at classification or feature detection tasks that require tactile discrimination abilities similar to those seen in whiskered animals. Previous work in this area has been reviewed in Fox et al. [5] and Prescott et al. [4]. In the current study we sought to examine the capacity of the BIOTACT sensor to simultaneously extract two different stimulation parameters: the horizontal (axial) distance to the contacted surface and the texture of that surface, with and without whisking modulation using RCP. To evaluate the effectiveness of the BIOTACT sensor in this discrimination task, we tested two different classification methods that we have developed for use with artificial vibrissal signals, one template-based [5], [31], [32]), the other using ‘naïve’ Bayes [33], [34]). Here we describe the experimental set-up used to generate a  $3 \times 3 \times 3$  (axial distance, texture, RCP) training and test (validation) data sets. We then briefly describe the two classification algorithms and the results of applying these to the BIOTACT sensor data.

### B. Texture Classification Experiments

A set of textured surfaces were fixed in a vertical plane and rigidly attached to the robot arm’s support post. The arm trajectory was pre-programmed to bring the front of the sensor to within a specified horizontal axial distance from the surface (5mm, 10mm or 15mm) with the two rows of whiskers aligned in a horizontal plane. Figure 4 shows a horizontal section through the sensor in its test configuration. All experiments were carried out with a whisk frequency ( $f_W$ ) of 2Hz. This is somewhat slower than the whisking frequency of rats (dominant frequency 8Hz [10]), but this is not unreasonable given the greater length of our whiskers (see section II-B). The choice of the 2Hz frequency is fairly arbitrary however, and limited testing at other whisking frequencies has not revealed

that this parameter is critical in achieving successful texture classification.

Three different textures have been used as discriminanda, a smooth plastic surface and two grades of commercial abrasive (3M silicon carbide ‘Wetordry Tri-M-ite’) see Table I. The latter surfaces were chosen to give a direct comparison with the whisking mobile robot “Whiskerbot” texture classification reported in Fox et al. [5].

TABLE I  
TEXTURED (ABRASIVE) SURFACES

ISO Grade	average particle diameter ( $\mu\text{m}$ )
P240	58.5
P600	25.8

The combination of three distances and three textures gave a total of nine distinct classes to be discriminated between.

We also present results comparing three different whisking strategies :-

#### Unmodulated

The whisker pattern generator output, unperturbed by feedback from sensors.

#### RCP7

Motor drive signal modulated with RCP, using a moderate gain factor ( $\sigma_z = 0.7$ , see equation 10)

#### RCP9

Motor drive signal modulated with RCP, using a stronger gain factor ( $\sigma_z = 0.9$ , see equation 10)

The purpose of this experiment was to determine whether RCP modulation was effective in improving the accuracy and robustness of classification and not to determine optimal values of these parameters. As such we chose values which we knew would be large enough to have a clearly visible effect on the output waveforms and small enough to prevent the biphasic whisking effect seen in simulation in figure 8.

#### C. Stationary Naïve Bayesian Classification

Bayesian classification involves recording the likelihoods of measurements from example sensory data. Given new test data, these likelihoods are used with Bayes’ rule to calculate the posterior probability of the test data being drawn from each trained class. The class with the largest posterior is most probable.

Here a stationary naïve Bayes classifier was used that had previously been demonstrated as an effective classifier of texture data [33], [34]. A naïve version of Bayes’ rule, in which the measurements are assumed to be statistically independent is used, along with an assumption of identical likelihoods over time, to calculate the posterior probability for each class of training data.

Briefly, the training data is used to estimate the log-probability distributions  $\log P_w(x_i|C_l)$  (log-likelihoods) of each sensor measurement  $x_i$  occurring. Measurements were quantized into one hundred equal-width intervals that spanned the entire data range of each whisker, then the resulting histogram of sensor measurements smoothed with a Gaussian

of width 5 intervals to correct for sampling errors and normalizing by the number of samples to give the likelihood. This led to  $n_w \times n_C$  log-likelihood functions, for each of the  $n_w = 12$  whisker inputs (two sensor directions for each of the six whiskers) and  $n_C = 9$  texture/distance classes.

Then, for each validation trial, the classification was achieved using naïve Bayes rule to calculate the nine posterior probabilities for each of the texture/distance classes, representing that the measurements were drawn from the twelve likelihoods for each of these possible classes. These posterior probabilities were calculated from the stationary naïve Bayes’ rule,

$$\log P(C_l|x_1, \dots, x_n) = \sum_{w=1}^{12} \sum_{i=1}^n \log P_w(x_i|C_l). \quad (15)$$

for flat priors, a stationary likelihood and the ‘naïve’ assumption of statistical independence. The classification is given by the largest log-posterior for each validation trial,

$$T = \arg \max_{T_l} \log P(C_l|x_1, \dots, x_n), \quad (16)$$

The utility of the stationary naïve Bayes rule is that it greatly simplifies the process of calculating the posteriors to an algorithm that is linear sum over log-likelihoods. Then the classification is similar in algorithmic complexity to a linear perceptron. Hence the classification is extremely fast, with real-time performance easily achievable on a standard PC.

#### D. Sum-of-squares Template-based Classification

Template based classification involves recording example sensory data as templates during a training phase, and comparing the stored templates to new data during the test phase. A template based classifier has been shown to be successful in discriminating whisker contacts of varying radial distance and speed [31]. Template based classification involves recording example sensory data as templates during a training phase, and comparing the stored templates to novel data during the test phase. By systematically comparing the novel data to signals encountered previously, a classification can be made by declaring which of the stored templates the novel signal is most similar to. This approach is straightforward to implement, and requires very little computation or pre-processing of the signal.

It has been shown previously that texture discrimination is dependent on whisker movement [35], and surface position [5]. In the present study each template corresponds to a texture-distance pair. Classification based on these templates is therefore simultaneous classification of both the texture and distance to contact. From the training data set an array of templates were generated by storing the average of the signals for each whisker in each class in the training set. This gave rise to 9 sets of 12 templates. During the test phase, trials were taken at random from the test set as inputs to the classifier. An element-wise sum of squared errors calculation was made between the input  $I$  and each template  $T_i$ ,

$$e(T_i) = \sum_{t=1}^n (I(t) - T_i(t))^2. \quad (17)$$

where  $n$  is the length of the template, in samples. A sum of errors from the 12 templates in each set were taken, and compared across the 9 classes. The class with the lowest total sum of squared errors was determined the winner, and a recording was made in an output array of the estimated texture and distance to contact of the input trial.

### E. Classification Performance

*1) Overall classification performance (unmodulated whisking dataset):* The hit rates over multiple validation trials were first calculated for the unmodulated whisking data set. From one to eight training whisks were used. Because a total of twelve (training and validation) whisks were measured, from  $11 \times 9$  to  $4 \times 9$  single whisks remained for validation over all nine texture/distance classes. The hit rate for each whisk number was then plotted against the number of training whisks (Figs. 10(a) and 11(a), solid black lines). Both classifiers show classification accuracy increasing with numbers of training whisks and reaching a maximum after 4 or 5 training whisks. Thereafter, increasing the number of whisks leads to similar performance.

*2) Comparative performance of unmodulated whisking, RCP7 and RCP9 datasets:* The unmodulated whisking dataset discussed in the preceding study was compared with results from the RCP datasets. Hit rates for each whisk number are plotted in figures 10(a) and 11(a), dashed and dotted lines.

For both classifiers, the RCP modulated whiskers give higher hit rates after one or two training whisks than the unmodulated, with RCP7 giving the highest accuracy. However, the two classifiers behave differently as the number of training whisks increases; using the stationary Bayesian method RCP7 continues increasing, reaching 100% accuracy after 7 training whisks, whereas with the template classifier, RCP7 shows little improvement and RCP9 begins to lose accuracy with increased training but suddenly improves after 6 training whisks.

*3) Classification performance for just textures or distances (unmodulated whisking dataset):* Classifiers for texture or distance (three classes of each) were then constructed by concatenating all training data for each distance or each texture. (Equivalently, the likelihoods could be averaged.) Once again, the number of training whisks was varied from one to eight and the hit rates plotted against whisk number (Figures 10(b),(c) and 11(b),(c) solid lines).

Using the stationary Bayesian method, classification for both features again reached high accuracy after about three/four training whisks. Roughly speaking, the hit rate for the single classifier texture/distance classifier was about equal to multiplying the hit rates for the individual classifiers, so there was no advantage apparent from considering either the single 9-class method or the double 3-class methods to distinguish both texture and distance. It should be noted that the double method is more efficient computationally, because a total of six classes are considered rather than nine.

The template-based method performed similarly on the distance classification task but only reached 75% hit rate on the texture classification.

*4) Comparative performance for just textures or distances of unmodulated whisking, RCP7 and RCP9 datasets:* Finally, the single-classifiers of texture or distance were applied to the RCP7 and RCP9 datasets and the hit rate plotted against training whisk number (Figures 10(b),(c) and 11(b),(c) dashed and dotted lines).

With the stationary Bayesian method, the same pattern of RCP7 being the best classifier, followed by RCP9 and then unmodulated whisking was again found, with the classification performance reaching its maximum at four whisks.

With the template-based method, RCP9 gave higher classification accuracy in texture classification. This was also the case in distance classification with less than 3 training whisks, but RCP modulated whisking resulted in lower accuracy than unmodulated with more training contacts.

## V. DISCUSSION

The design of tactile sensor systems for robots has taken inspiration from mammalian whiskers (see [4]), and from insect antennae (see e.g. [36], [37]), since at least the 1980s. However, most work in this field has not specifically addressed the contribution of sensor motion to the problem of tactile discrimination. Earlier work by the current authors identified characteristic features of active sensing control in the whisker movement of rats [17], [18] and showed that these could be incorporated into artificial vibrissal systems for robots [20], [21]. In the current study we extended this work to directly examine the impact of active control on a two-dimensional (texture  $\times$  distance) sensory discrimination task. Based on these early results we appear to see an advantage for active control (rapid cessation of protraction – RCP) for classification after fewer training whisk cycles, particularly when using the stationary naïve Bayes method. This outcome is perhaps surprising in that RCP tends to reduce rather than increase the duration of contact between the whisker and the surface. It therefore suggests that the benefit of RCP may be to increase the repeatability of whisker-surface contacts. The advantage is not clearly demonstrated when using the template based method and more than 2 training whisks; under which circumstances classification of distance was actually less accurate when RCP modulation was applied. Further experiments both with artificial vibrissae and perhaps, using *in vivo* electrophysiology in animals, could usefully investigate the specific consequence of this aspect of control that might lead to improved discriminative capabilities. One of the advantages of the BIOTACT Sensor, over our earlier work on artificial vibrissal systems, is that the whiskers are individually actuated; therefore, sensor movement can potentially be modulated by sensory feedback on a per-whisker basis. Although we have yet to explore this possibility, our experimental work with rats suggests that whisker velocity can be differentially controlled for more anterior and posterior whiskers in a manner that affects the angular spread of the whiskers [18]. We also found a difference of up to 5 milliseconds in the timing of RCP, with posterior whiskers beginning to retract later than more anterior ones [18]. The artificial whisker results presented above suggest that such differences, whilst subtle, could be

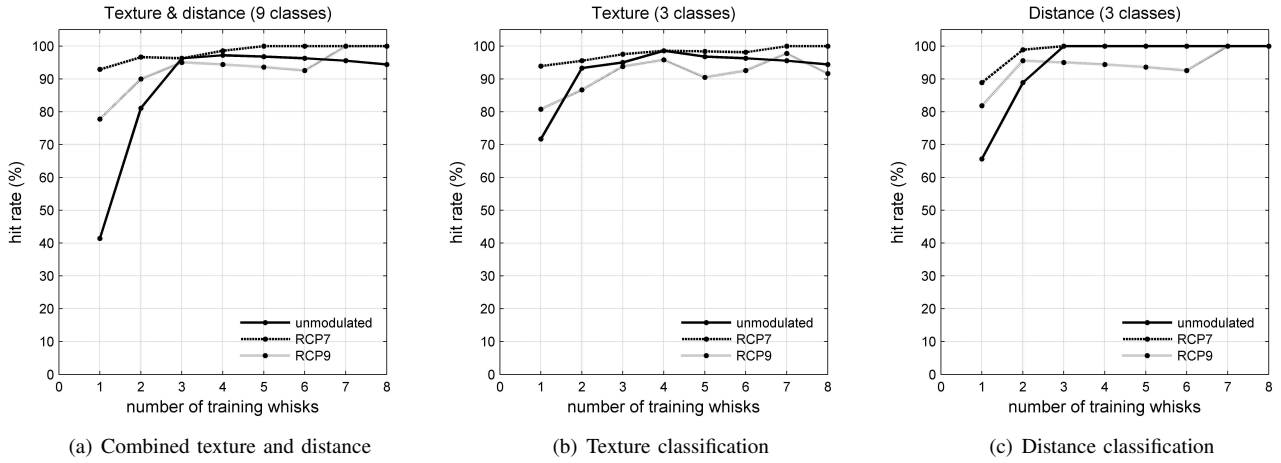


Fig. 10. Classification performance using naïve Bayes.

Panel A compares the performance of the unmodulated, RCP7 and RCP9 datasets for classifying both texture and distance together. Panels B and C are analogous to panel A, but for a single classification of either texture or distance. Classification accuracy is measured by hit rate, which is the ratio of successful classifications to validation whiskers.

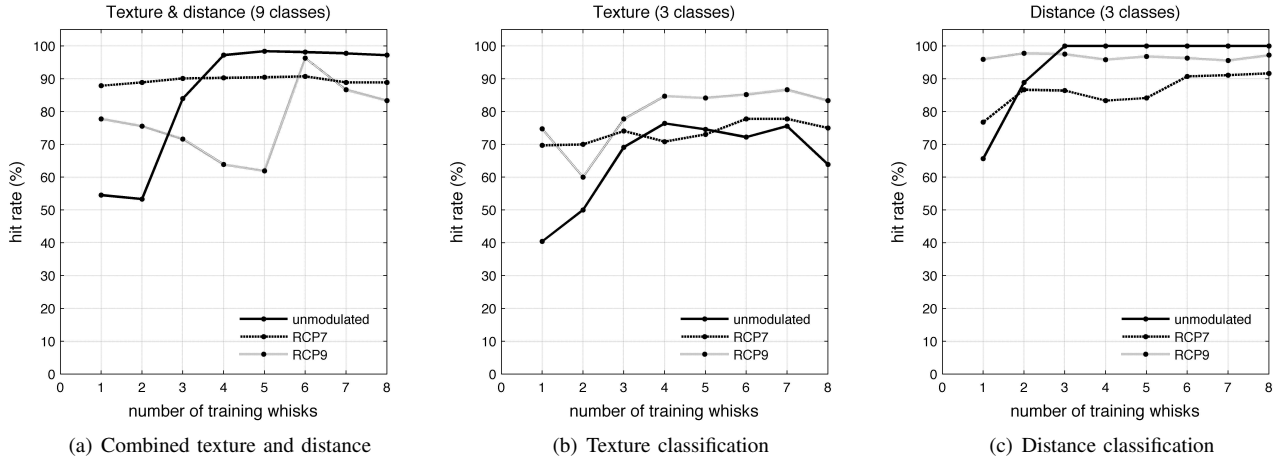


Fig. 11. Classification performance using template based classifier.

Classification accuracy is measured by hit rate, which is the ratio of successful classifications to validation whiskers.

impacting on the discrimination capabilities of the whiskers. Since the experiments described here used only symmetric contacts with a vertical surface, we have also yet to investigate or quantify the impact of other aspects of active whisking control (particularly contact-induced asymmetry) on sensory processing.

It has been shown previously that whisker-based texture discrimination is critically dependent on whisker-object contact geometry [5]. In the current study, inspection of the raw signals for each class reveals greater within class variation for contacts with a given texture than at a given distance. This is because contacts at different distances result in stereotypical macroscopic changes in whisker deflection amplitude [32], whereas texture-dependent features involve smaller and more variable deflections of the whisker (either by their direct contact with random particles on the rough surface or by an oscillatory ‘ringing’ of the whisker as it draws away from the surface). This variation could perhaps explain why the template-based classifier considered here did not generalize well across conditions when attempting to classify texture,

compared to the stationary Naïve Bayes classifier (compare figures 10(b) and 11(b)).

Figure 12 shows single-whisker time histories of the signals from one of the smaller whiskers contacting the smooth and p240 textures at the same distance, together with spectrograms computed using the reassigned Gabor time-frequency representation [38]. Although the effect of RCP can be clearly seen in the time history, the differences between textures are more subtle.

Further support that the time-independence of a classifier can lend it robustness in certain circumstances is given by an equivalence between the template classifier and a form of Naïve Bayes classifier. Because the considered template classifier uses a sum-of-squares error function, it is equivalent to a log-product of independent noise terms that satisfy the Naïve Bayes definition,

$$\sum_{t=1}^N (I(t) - T_i(t))^2 = -\log \prod_{t=1}^N \frac{1}{Z_i} \exp -\frac{(I(t) - T_i(t))^2}{2\sigma^2} - c, \quad (18)$$

for constants  $\sigma = 1/2$ ,  $c = \sum_i \log Z_i$  and  $Z_i$  area-terms

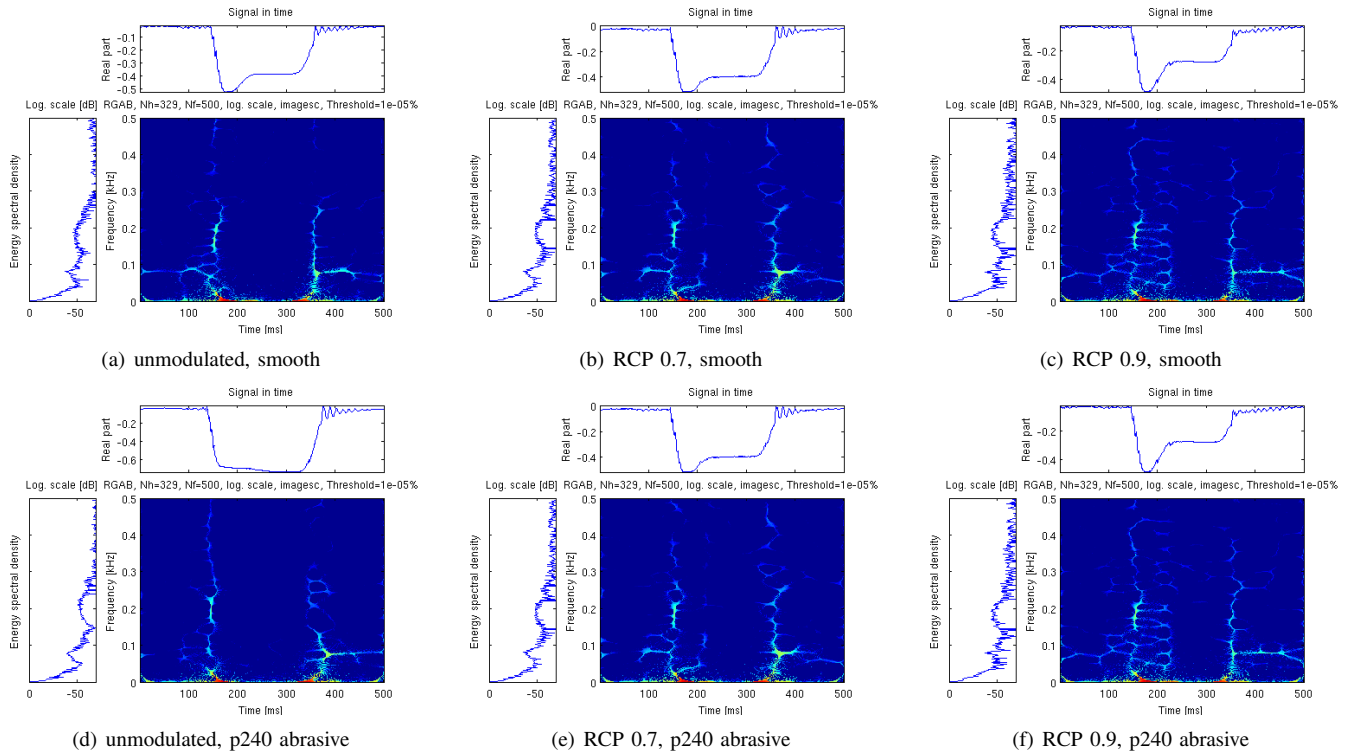


Fig. 12. Spectral analysis comparing response of smooth and textured (p240) surfaces with and without RCP modulation. Spectrograms computed using reassigned Gabor time-frequency representation (Time Frequency Toolbox (<http://tftb.nongnu.org>) `tfrgab` function)

cancelling with *c*. We can then consider the differences between these two forms of Naïve Bayes. The above Naïve Bayes formulation of the template classifier assumes varying noise distributions over time *t* and can thus be interpreted as a time-dependent Naïve Bayes classifier. In contrast, the Naïve Bayes considered earlier in this paper was stationary, supporting that time-dependence/independence is the principle difference between the two classifiers considered here. That being said, in some circumstances the simplifying assumption of time-independence may be a hindrance, for example when the phases of the oscillations are crucial to the classification. Future work could investigate new forms of Naïve Bayes rules combining useful properties of both methods. The success of Naïve Bayes classification is encouraging and suggests that this relatively simple technique could potentially be a useful tool for other discrimination tasks involving time series data.

One of the goals in designing this first generation BIOTACT Sensor was to produce a modular unit that could be flexibly assembled into different configurations. The first configuration investigated was chosen to be a simple, radially symmetric cone with a small number of whiskers. This configuration clearly does not match the vibrissal system of the rat in a number of ways, one important consequence of which is that the sensory “surface” formed by the whiskers tips at full protraction does not form a broad field in front of the sensing device in the manner observed in animal (compare Figures 1 and 2 for example). A second generation system, currently under construction, is being developed to specifically address this limitation. It will also incorporate an array of shorter, more closely spaced, unactuated *microvibrissae*, again

based on the morphology of the rat which has a similar array on the frontal part of the snout and around its mouth and which have been shown to play a key role in object discrimination [9]. In addition to a more biomimetic sensor morphology, we also plan to improve aspects of the sensory processing. For instance, we have shown that, in the task of detecting whisker-surface contacts, sensor noise, due to the movement of the whiskers alone, can generate spurious false positives [39]. To address this problem, we previously developed an adaptive filtering algorithm that uses a copy of the motor control signal to predict movement-related sensory noise, such that cleaned-up signals (from which the predicted noise is subtracted) avoid the problem of spurious contacts. The same filter will likely prove useful in discrimination tasks such as the distance/texture problem considered above. Interestingly, the algorithm employed for adaptive filtering was modeled on the microcircuitry of the mammalian cerebellum, which, in rats, is known to be heavily involved in processing vibrissal signals.

A long-term ambition of our research is to identify the computations that are carried out in the rat brain when the animal is engaged in tasks that involve tactile discrimination. The classification methods, described above, are not specifically derived from considerations of how vibrissal processing mechanisms in the rat brain may operate. However, if we are able to devise effective classifiers whose capabilities match those of the rat, these can, in future, be used to inform hypotheses about the biological system that may be testable using neurophysiological data.

Most tactile sensors for robots are binary devices that do

little more than detect whether or not a contact has happened. Biology shows us that this is a modality with considerably greater potential. In order to make the most of tactile sensing we believe that the biomimetic route, focusing particularly on the role of active control, can inspire technologies that will provide future robots with a sense of touch to parallel, or even surpass, that of animals. The BIOTACT Sensor, described in this article, is we hope a useful step towards this longer-term goal.

## REFERENCES

- [1] R. Bajcsy, "Active perception," *Proceedings of the IEEE*, vol. 76, pp. 996–1005, 1988.
- [2] S. J. Lederman and R. L. Klatzky, "Extracting object properties through haptic exploration," *Acta Psychol (Amst)*, vol. 84, no. 1, pp. 29–40, 1993.
- [3] T. Prescott, B. Mitchinson, and R. Grant, "Vibrissal behavior and function," *Scholarpedia*, 2010, in Press.
- [4] T. Prescott, M. Pearson, B. Mitchinson, J. Sullivan, and A. Pipe, "Whisking with robots from rat vibrissae to biomimetic technology for active touch," *IEEE Robotics and Automation Magazine*, vol. 16, no. 3, pp. 42–50, 2009.
- [5] C. Fox, B. Mitchinson, M. Pearson, A. Pipe, and T. Prescott, "Contact type dependency of texture classification in a whiskered mobile robot," *Autonomous Robots*, vol. 26, pp. 223–239, 2009.
- [6] A. S. Ahl, "The role of vibrissae in behavior - a status review," *Veterinary Research Communications*, vol. 10, no. 4, pp. 245–268, 1986. [Online]. Available: <http://dx.doi.org/10.1007/BF02213989>
- [7] B. Mitchinson, K. N. Gurney, P. Redgrave, C. Melhuish, A. G. Pipe, M. Pearson, I. Gilhespy, and T. J. Prescott, "Empirically inspired simulated electro-mechanical model of the rat mystacial follicle-sinus complex," *Proc R Soc Lond B Biol Sci*, vol. 271, no. 1556, pp. 2509–2516, Dec 2004.
- [8] D. N. Hill, R. Bermejo, H. P. Zeigler, and D. Kleinfeld, "Biomechanics of the Vibrissa Motor Plant in Rat: Rhythmic Whisking Consists of Triphasic Neuromuscular Activity," *J. Neurosci.*, vol. 28, no. 13, pp. 3438–3455, 2008.
- [9] M. Brecht, B. Preilowski, and M. M. Merzenich, "Functional architecture of the mystacial vibrissae," *Behavioural Brain Research*, vol. 84, no. 1-2, pp. 81–97, 1997.
- [10] G. Carvell and D. Simons, "Biometric analyses of vibrissal tactile discrimination in the rat," *Journal of Neuroscience*, vol. 10, no. 8, pp. 2638–2648, 1990.
- [11] B. Mitchinson, T.-S. Chan, J. Chambers, M. Pearson, M. Humphries, C. Fox, K. Gurney, and T. J. Prescott, "BRAHMS: Novel middleware for integrated systems computation," *Advanced Engineering Informatics*, vol. 24, no. 1, pp. 49–61, 2010.
- [12] C. M. Williams and E. M. Kramer, "The advantages of a tapered whisker," *PLoS ONE*, vol. 5, no. 1, p. e8806, 01 2010. [Online]. Available: <http://dx.doi.org/10.1371/journal.pone.0008806>
- [13] M. J. Hartmann, N. J. Johnson, R. B. Towal, and C. Assad, "Mechanical characteristics of rat vibrissae: Resonant frequencies and damping in isolated whiskers and in the awake behaving animal," *The Journal of Neuroscience*, vol. 23, no. 16, pp. 6510 –6519, Jul. 2003. [Online]. Available: <http://www.jneurosci.org/content/23/16/6510.abstract>
- [14] P. Gao, R. Bermejo, and H. P. Zeigler, "Whisker Deafferentation and Rodent Whisking Patterns: Behavioral Evidence for a Central Pattern Generator," *J. Neurosci.*, vol. 21, no. 14, pp. 5374–5380, 2001.
- [15] R. W. Berg and D. Kleinfeld, "Rhythmic whisking by rat: Retraction as well as protraction of the vibrissae is under active muscular control," *J. Neurophysiol.*, vol. 89, no. 1, pp. 104–117, Jan 2003.
- [16] R. B. Towal and M. J. Hartmann, "Right-left asymmetries in the whisking behavior of rats anticipate head movements," *J. Neurosci.*, vol. 26, no. 34, pp. 8838–46, 2006.
- [17] B. Mitchinson, C. J. Martin, R. A. Grant, and T. J. Prescott, "Feedback control in active sensing: rat exploratory whisking is modulated by environmental contact," *Royal Society Proceedings B*, vol. 274, no. 1613, pp. 1035–1041, 2007.
- [18] R. A. Grant, B. Mitchinson, C. W. Fox, and T. J. Prescott, "Active touch sensing in the rat: Anticipatory and regulatory control of whisker movements during surface exploration," *Journal of Neurophysiology*, vol. 101, pp. 862–874, 2009.
- [19] B. Mitchinson, M. Pearson, C. Melhuish, and T. J. Prescott, "A model of sensorimotor co-ordination in the rat whisker system," in *From Animals to Animats 9: Proceedings of the Ninth International Conference on Simulation of Adaptive Behaviour*, 2006, pp. 77–88.
- [20] M. J. Pearson, A. G. Pipe, C. Melhuish, B. Mitchinson, and T. J. Prescott, "Whiskerbot: A Robotic Active Touch System Modeled on the Rat Whisker Sensory System," *Adaptive Behavior*, vol. 15, no. 3, pp. 223–240, 2007. [Online]. Available: <http://adb.sagepub.com/content/15/3/223.abstract>
- [21] M. J. Pearson, B. Mitchinson, J. Welsby, T. Pipe, and T. Prescott, "Scratchbot: Active tactile sensing in a whiskered mobile robot," in *From Animals to Animats 11*, ser. Lecture Notes in Computer Science, S. Doncieux, B. Girard, A. Guillot, J. Hallam, J.-A. Meyer, and J.-B. Mouret, Eds. Springer Berlin / Heidelberg, 2010, vol. 6226, pp. 93–103.
- [22] B. Mitchinson, M. Pearson, T. Pipe, and T. J. Prescott, "Biomimetic robots as scientific models: A view from the whisker tip," in *Neuromorphic and Brain-based Robots*, J. Krichmar, Ed. MIT Press, 2010, in press.
- [23] R. B. Towal and M. J. Z. Hartmann, "Variability in Velocity Profiles During Free-Air Whisking Behavior of Unrestrained Rats," *J Neurophysiol*, vol. 100, no. 2, pp. 740–752, 2008. [Online]. Available: <http://jn.physiology.org/cgi/content/abstract/100/2/740>
- [24] M. Diamond, M. von Heimendahl, and E. Arabzadeh, "Whisker-mediated texture discrimination," *PLoS Biol.*, vol. 6, no. 8, 2008.
- [25] F. Anjum, H. Turni, P. G. Mulder, J. van der Burg, and M. Brecht, "Tactile guidance of prey capture in etruscan shrews," *Proc Natl Acad Sci U S A*, vol. 103, no. 44, pp. 16 544–16 549, 2006.
- [26] E. Ahissar and P. M. Knutson, "Object localization with whiskers," *Biol Cybern*, vol. 98, no. 6, pp. 449–458, 2008.
- [27] E. Guic-robles, G. Guajardo, and C. Valdivieso, "Rats can learn a roughness discrimination using only their vibrissal system," *Behavioural Brain Research*, vol. 31, pp. 285–289, 1989.
- [28] E. Guic-robles, W. M. Jenkins, and H. Bravo, "Vibrissal roughness discrimination is barrelcortex-dependent," *Behavioural Brain Research*, vol. 48, no. 2, pp. 145–152, 1992.
- [29] J. Hipp, E. Arabzadeh, E. Zorzin, J. Conradt, C. Kayser, M. E. Diamond, and P. Konig, "Texture signals in whisker vibrations," *J Neurophysiol*, vol. 95, no. 3, pp. 1792–9, 2006.
- [30] J. Wolfe, D. N. Hill, S. Pahlavan, P. J. Drew, D. Kleinfeld, and D. E. Feldman, "Texture coding in the rat whisker system: slip-stick versus differential resonance," *PLoS Biol.*, vol. 6, no. 8, p. e215, 2008.
- [31] M. Evans, C. W. Fox, M. J. Pearson, and T. J. Prescott, "Tactile discrimination using template classifiers: Towards a model of feature extraction in mammalian vibrissal systems," in *Proceedings of the 11th International Conference on Simulation of Adaptive Behaviour*, 2010.
- [32] ———, "Whisker-object contact speed affects radial distance estimation," in *Proceedings 2010 IEEE International Conference on Robotics and Biomimetics (ROBIO)*. Available: [Preprint: http://dl.dropbox.com/u/2933960/Evans.Robio.2010.pdf](http://dl.dropbox.com/u/2933960/Evans.Robio.2010.pdf), 2010.
- [33] N. F. Lepora, M. Evans, C. W. Fox, M. E. Diamond, K. N. Gurney, and T. J. Prescott, "Naive bayes texture classification applied to whisker data from a moving robot," in *IEEE Proceedings of IJCN*, Apr 27 2010, pp. 1–8.
- [34] N. F. Lepora, M. Pearson, B. Mitchinson, M. Evans, C. Fox, T. Pipe, K. Gurney, and T. Prescott, "Naive bayes novelty detection for a moving robot with whiskers," in *IEEE Proceedings of ROBIO 2010*, 2010, (in press) Preprint available ([www.lepora.com](http://www.lepora.com)).
- [35] M. Evans, C. W. Fox, M. J. Pearson, and T. J. Prescott, "Spectral template based classification of robotic whisker sensor signals in a floor texture discrimination task," in *Proceedings of Towards Autonomous Robotic Systems (TAROS 2009)*, T. Kyriacou, U. Nehmzow, C. Melhuish, and M. Witkowski, Eds., 2009, pp. 19–24.
- [36] M. Kaneko, N. Kanayama, and T. Tsuji, "Active antenna for contact sensing," *IEEE Trans. Robotics and Automation*, vol. 14, no. 2, pp. 278–291, 1998.
- [37] A. Lamperski, O. Loh, B. Kutscher, and N. Cowan, "Dynamical wall following for a wheeled robot using a passive tactile sensor," in *Robotics and Automation, 2005. ICRA 2005. Proceedings of the 2005 IEEE International Conference on*, 2005, pp. 3838 – 3843.
- [38] P. Flandrin, F. Auger, and E. Chassande-Mottin, "Time-frequency reassignment: from principles to algorithms," in *Applications in Time Frequency Signal Processing*, A. Papandreou-Suppappola, Ed. Boca Raton, FL: CRC Press, 2003, pp. 179–203.
- [39] S. A. Anderson, M. J. Pearson, A. G. Pipe, T. J. Prescott, P. Dean, and J. Porrill, "Adaptive cancellation of self-generated sensory signals in a whisking robot," *IEEE Transactions on Robotics*, pp. 1–12, Aug 2010.